Nuclear structure of Te isotopes beyond neutron magic number $N = 82$

B. Moon,[1,2] A. Jungclaus,[3,*] H. Naïdja,[4] A. Gargano,[5] R. Lozeva,[6,7] C.-B. Moon,[1,†] A. Odahara,[8] G. S. Simpson,[9] S. Nishimura,[2] F. Browne,[2,10] P. Doornenbal,[2] G. Gey,[9,11,2] J. Keatings,[12] G. Lorusso,[2] Z. Patel,[2,13] S. Rice,[2,13] M. Si,[7] L. Sinclair,[2,14] P.-A. Söderström,[15,2] T. Sumikama,[2] J. Taprogge,[3,16,2] H. Watanabe,[2] J. Wu,[2,17] Z. Y. Xu,[18] A. Yagi,[8] D. S. Ahn,[2,19] H. Baba,[2] F. L. Bello Garrote,[20] S. Bönig,[21] R. Daido,[8] J. M. Daugas,[22] F. Didierjean,[6] F. Drouet,[9] Y. Fang,[8] N. Fukuda,[2] R. Gernhäuser,[23] B. Hong,[24,25] E. Ideguchi,[26] S. Ilieva,[21] N. Inabe,[2] T. Ishigaki,[8] T. Isobe,[2] H. S. Jung,[27] D. Kameda,[2] I. Kojouharov,[28] T. Komatsubara,[2] T. Kröll,[21] T. Kubo,[2] N. Kurz,[28] Y. K. Kwon,[29] C. S. Lee,[27] P. Lee,[27] Z. Li,[17] A. Montaner-Pizá,[30] S. Morimoto,[8] K. Moschner,[31] D. Mücher,[23] D. Murai,[32] M. Niikura,[2,18] H. Nishibata,[8] I. Nishizuka,[33] R. Orlandi,[34,35] H. Sakurai,[2,18] H. Schaffner,[28] Y. Shimizu,[2] K. Steiger,[23] H. Suzuki,[2] H. Takeda,[2] K. Tshoo,[29] Zs. Vajta,[36] A. Wendt,[31] R. Yokoyama,[37] and K. Yoshinaga[38]

[1] *Center for Exotic Nuclear Studies, Institute for Basic Science, Daejeon 34126, Republic of Korea*
[2] *RIKEN Nishina Center, Wako, Saitama 351-0198, Japan*
[3] *Instituto de Estructura de la Materia, CSIC, E-28006 Madrid, Spain*
[4] *Laboratoire de Physique Mathematique et Subatomique, Constantine 1 University, Constantine 25000, Algeria*
[5] *Istituto Nazionale di Fisica Nucleare, Complesso Universitario di Monte S. Angelo, I-80126 Napoli, Italy*
[6] *IPHC, CNRS/IN2P3 and University of Strasbourg, F-67037 Strasbourg Cedex 2, France*
[7] *Université Paris-Saclay, IJCLab, CNRS/IN2P3, F-91405 Orsay, France*
[8] *Department of Physics, Osaka University, Osaka 560-0043, Japan*
[9] *LPSC, Université Joseph Fourier Grenoble 1, CNRS/IN2P3, Institut National Polytechnique de Grenoble, F-38026 Grenoble Cedex, France*
[10] *School of Computing, Engineering and Mathematics, University of Brighton BN2 4GJ, United Kingdom*
[11] *Institut Laue-Langevin, B.P. 156, F-38042 Grenoble Cedex 9, France*
[12] *School of Engineering, University of the West of Scotland, Paisley PA1 2BE, United Kingdom*
[13] *Department of Physics, University of Surrey, Guildford, GU2 7XH, United Kingdom*
[14] *Department of Physics, University of York, Heslington, York YO10 5DD, United Kingdom*
[15] *Extreme Light Infrastructure-Nuclear Physics (ELI-NP), 077125 Bucharest-Măgurele, Romania*
[16] *Departamento de Física Teórica, Universidad Autónoma de Madrid, E-28049 Madrid, Spain*
[17] *School of Physics and State key Laboratory of Nuclear Physics and Technology, Peking University, Beijing 100871, China*
[18] *Department of Physics, University of Tokyo, Tokyo 113-0033, Japan*
[19] *Korea Basic Science Institute (KBSI), Daejeon 34133, Republic of Korea*
[20] *Department of Physics, University of Oslo N-0316, Norway*
[21] *Institut für Kernphysik, Technische Universität Darmstadt, D-64289 Darmstadt, Germany*
[22] *CEA, DAM, DIF, F-91297 Arpajon Cedex, France*
[23] *Physik Department E12, Technische Universität München, D-85748 Garching, Germany*
[24] *Department of Physics, Korea University, Seoul 02841, Republic of Korea*
[25] *Center for Extreme Nuclear Matters (CENuM), Korea University, Seoul 02841, Republic of Korea*
[26] *RCNP, Osaka University, Osaka 567-0047, Japan*
[27] *Department of Physics, Chung-Ang University, Seoul 06974, Republic of Korea*
[28] *GSI Helmholtzzentrum für Schwerionenforschung GmbH, D-64291, Darmstadt, Germany*
[29] *Rare Isotope Science Project, Institute for Basic Science, Daejeon 34047,Republic of Korea*
[30] *Instituto de Física Corpuscular, CSIC-Univ. of Valencia, E-46980 Paterna, Spain*
[31] *IKP, University of Cologne, D-50937 Cologne, Germany*
[32] *Department of Physics, Rikkyo University, Tokyo 172-8501, Japan*
[33] *Department of Physics, Tohoku University, Sendai, Miyagi 980-8578, Japan*
[34] *Instituut voor Kern- en StralingsFysica, K.U. Leuven, B-3001 Heverlee, Belgium*
[35] *Advanced Science Research Center, Japan Atomic Energy Agency, Tokai, Ibaraki, 319-1195, Japan*
[36] *Atomki, P.O. Box 51, Debrecen H-4001, Hungary*
[37] *Center for Nuclear Study, University of Tokyo, RIKEN Campus, Wako, Saitama 351-0198, Japan*
[38] *Department of Physics, Faculty of Science and Technology, Tokyo University of Science, 2641 Yamazaki, Noda, Chiba, Japan*

(Dated: March 4, 2021)

Newly observed decay schemes of the nuclei ^{137}Sb and ^{138}Sb are reported. The neutron-rich Sb isotopes were produced by the in-flight fragmentation of a ^{238}U primary beam with an energy of 345 MeV/nucleon. Several new excited states of ^{137}Te with tentatively assigned spin-parities of $(5/2^-)$, $(9/2^-)$, and $(7/2)$ have been established which play an important role in the evolution of neutron levels beyond $N = 82$. The study of the β decay of ^{138}Sb led to a considerable extension of the level

scheme of ^{138}Te including the identification of several non-yrast states. The structure of ^{137}Te and ^{138}Te is discussed on the basis of large-scale shell-model calculations performed using two different effective interactions.

I. INTRODUCTION

Nuclei around ^{132}Sn with the neutron magic number $N = 82$ play a significant role in nuclear structure and nuclear astrophysics. The region north-east of ^{132}Sn, in particular, provides crucial information on the nature of the nucleon-nucleon interactions. Moreover, this region is closely related to the rapid-neutron capture process, the so-called r-process, one of the nucleosynthesis mechanisms in the cosmos [1–3]. Therefore, the nuclear structure properties are essential to reproduce the r-process abundances and to understand the origin of the elements in the universe [3–5].

Among the nuclides in this region, tellurium (Te) with two protons above the shell closure at $Z = 50$ is of special interest. Particularly, the ^{136}Te isotope with one proton and one neutron pair outside the robust double magic ^{132}Sn core has attracted much attention of nuclear physicists for a long time [6–11]. Through Coulomb excitation experiments, the collective behavior of ^{136}Te is revealed to be dominated by the pair of valence neutrons [6–8]. Moreover, recent β-decay experiments established the collective behavior of the heavier Te isotopes ^{138}Te [12] and ^{140}Te [13], showing typical vibrational characters. Consequently, the neutron-rich Te isotopes are expected to have their own peculiar characteristics in terms of the collective motion, which is different from both the semi-magic character of the Sn isotopes [14] and the well-developed quadrupole and octupole deformations appearing in the Xe and Ba isotopes [15]. On the other hand, very limited experimental information is available for the odd-mass (A) Te isotopes beyond the neutron magic number of $N = 82$. Therefore, further investigations of the neutron-rich Te isotopes are important for a better understanding of the neutron shell evolution in this region.

In the present work, the β-decay schemes of ^{137,138}Sb and the level structures in the daughter nuclei ^{137,138}Te are reported. The latter are discussed in the context of large-scale shell-model calculations. Based on the comparison between the experimental and theoretical results, detailed structure information such as the neutron dominance is revealed.

II. EXPERIMENT PROCEDURE

Two individual experiments were performed at the Radioactive Isotope Beam Factory (RIBF) operated by the RIKEN Nishina Center for Accelerator-Based Science and the Center for Nuclear Study of the University of Tokyo. Secondary beams were produced by the in-flight fragmentation of ^{238}U primary beams at 345 MeV per nucleon, impinging on a ^{9}Be target [16]. Neutron-rich ^{137,138}Sb isotopes were selected in the first stage of the BigRIPS spectrometer and identified by the $B\rho$-ΔE-time-of-flight method along the second stage of the BigRIPS and the Zero-Degree Spectrometer [17]. One of the experiments is called the Te campaign since the BigRIPS and Zero-Degree Spectrometer were tuned on the ^{142}Te isotope. The other experiment is nominated the Sn campaign, in which the spectrometers were optimized for the transmission of ^{135}Sn. The numbers of the identified ^{137}Sb and ^{138}Sb ions from the Sn campaign were 1.3×10^5 and 5.6×10^5, respectively, while 5.0×10^3 ^{137}Sb and 1.4×10^5 ^{138}Sb ions were transmitted during the Te campaign.

The selected secondary beams were implanted into the Wide-range Active Silicon Strip Stopper Array for β and ion detection (WAS3ABi) [18], composed of multiple layers of 1-mm-thick double-sided silicon strip detectors (DSSSD) with an active area of 60×40 mm^2. The correlation between the implanted ions and the emitted β rays could be achieved based on the position resolution of WAS3ABi, since each Si layer consists of 60 vertical and 40 horizontal 1-mm wide strips. Five and eight layers of WAS3ABi were installed during the Te and Sn campaigns, respectively. The γ rays emitted from implanted ions were detected by the EUROBALL-RIKEN Cluster Array (EURICA), comprised of twelve cluster detectors with seven hexagonal-tapered high-purity germanium crystals each [19]. The γ-ray detection efficiencies without the add-back algorithm were 8.7(4)% and 6.7(3)% at 1 MeV for the Te and Sn campaigns, respectively, and the difference in the efficiencies was mainly from the different configuration of detectors.

III. EXPERIMENTAL RESULTS

III.1. Beta decay of ^{137}Sb

Collective band structures based on the $(7/2^-)$ ground state of ^{137}Te were established using spontaneous fission of ^{248}Cm [20]. In that work, only high-spin states were populated, so that the $(11/2^-)$ member of the ground-state band at an excitation energy of 608 keV is the level with the lowest spin whose decay could be observed. In the present work, for the first time, information on low-spin states in this nucleus, populated in the β decay of ^{137}Sb, is reported. Figure 1 shows the background-subtracted β-delayed γ-ray singles spectrum of ^{137}Sb. In order to identify the γ-ray transitions following the β decay of ^{137}Sb, singles spectra were obtained with two different time conditions, one with a gate in the prompt $(0 - 1500$ ms) and the other one with a gate in the de-

* andrea.jungclaus@csic.es
† cbmoon@ibs.re.kr

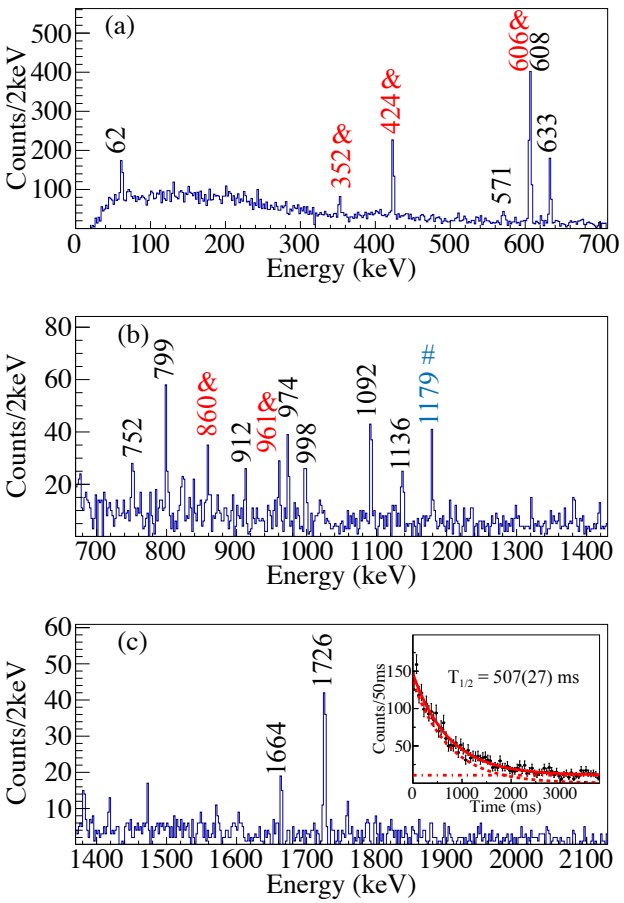

FIG. 1. Background-subtracted β-delayed γ-ray singles spectrum of ^{137}Sb. Black numbers represent the energies of the γ-ray transitions following β decay while red (blue) numbers marked by & (#) indicate transitions following the β-delayed emission of one (two) neutron(s). Several unlabelled peaks, such as in (b) and (c), could not be assigned due to their small statistics and absence of γ-γ coincidence information. The inset in (c) shows the half-life measurement of ^{137}Sb with gate on 606-, 608-, 633-, and 974-keV transitions.

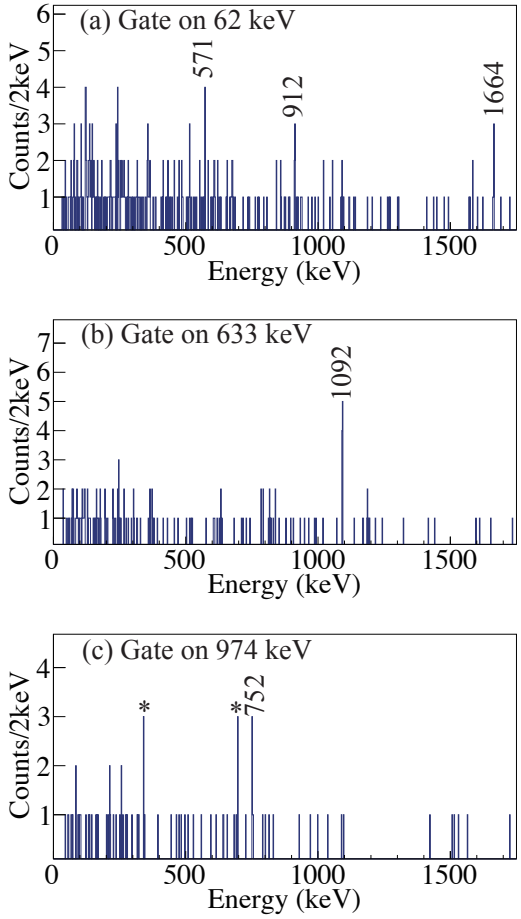

FIG. 2. γ-γ coincidence spectra for (a) the 62-, (b) the 633-, and (c) the 974-keV transition in ^{137}Te. Coincident transitions are indicated with their energies and contaminants are labeled with asterisks (*).

layed (2500 − 4000 ms) region. Here, the timing information is defined by the time-stamp correlation between the implanted ion and emitted β-ray events. Moreover, only events in which the ion and the β ray were detected in the same pixel of the WAS3ABi array were considered in order to improve the data quality by reducing the background. The assigned transitions are indicated with their energies in black for β decay, red for β-delayed one-neutron emission, and blue for β-delayed two-neutron emission. The half-life of ^{137}Sb was determined by gating on the 606-, 608-, 633-, and 974-keV transitions, as shown in an inset in Fig. 1(c). The fit was performed by using the maximum-likelihood method with a fit function composed of a single-component exponential decay and a constant background. The deduced half-life value, $T_{1/2}$=507(27) ms, is consistent with the value of 492(25) ms reported in the literature [21]. As shown in Fig. 2, the γ-γ coincidence method was applied to construct the level scheme of ^{137}Te. In addition, also γ-ray energy sums were used. The experimental information on the γ-ray transitions is summarized in Table I and Figure 3 illustrates the decay scheme of ^{137}Sb as established in the present work.

The ground state of ^{137}Sb is proposed to have a spin-parity of $(7/2^+)$ based on the following arguments. Firstly, the observation of the 608-keV transition is crucial. This transition decays from a $(11/2^-)$ state [20] and therefore suggests a minimum spin of 7/2 due to the selection rule. Secondly, the observed cascading γ-ray transitions in ^{136}Te, emitted following β-delayed neutron emission, show intensities similar to those in ^{134}Te following the decay of ^{135}Sb [22]. The reported neutron-feeding branching ratios are 21(3), 11(2), and 6(1)%, respectively, for the 2^+, 4^+, and 6^+ states of ^{134}Te, while in the present work absolute branching ratios of 10.0(27), 5.2(18), and 3.2(9)% for the same states in ^{136}Te were determined. Although differing by roughly a factor of two on the absolute scale, the relative intensities are very similar. If the spins of the ground states of ^{135}Sb and ^{137}Sb were different, significant differences between the relative

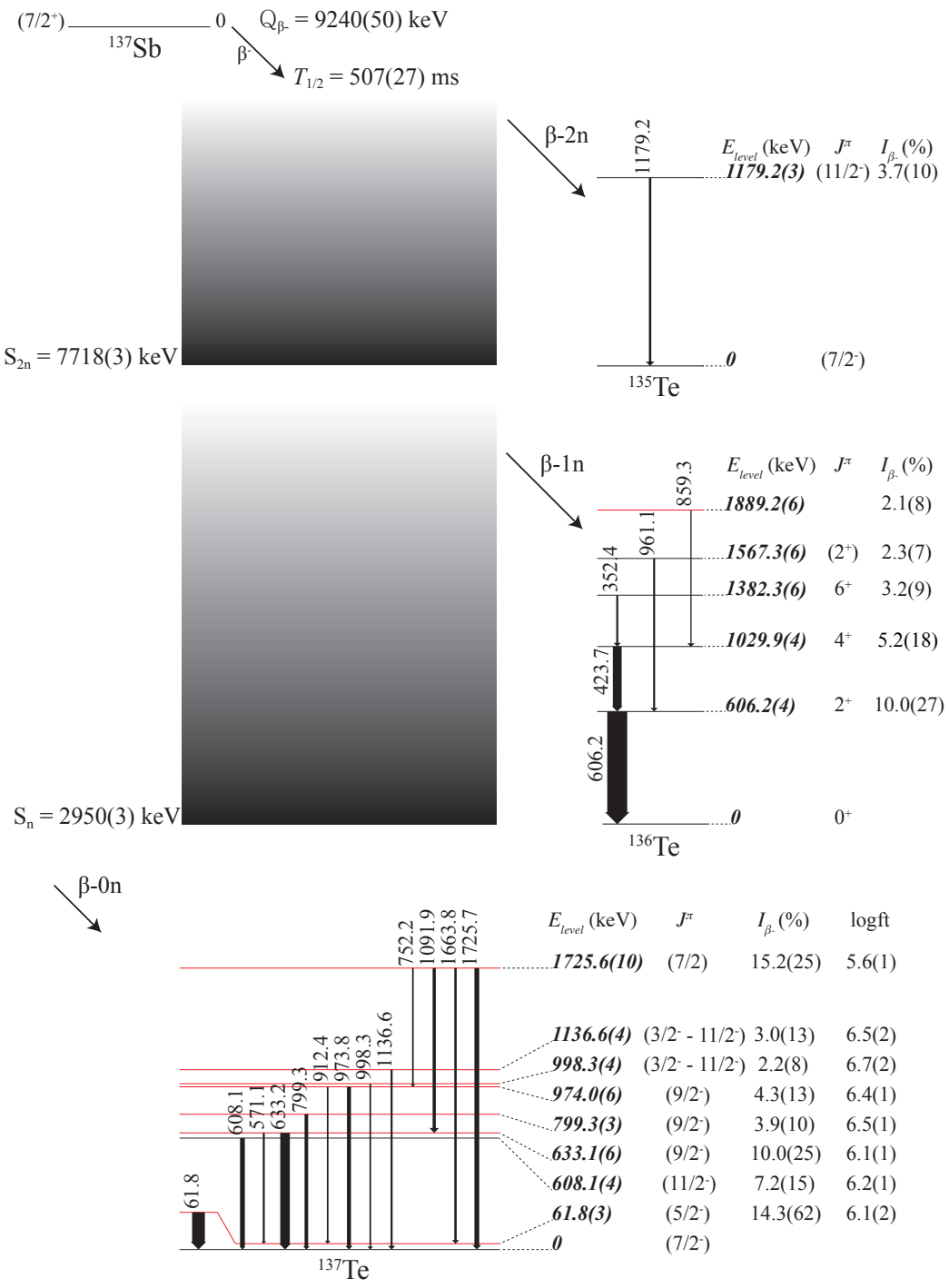

FIG. 3. β-decay scheme of ^{137}Sb. The half-life of the ground state of ^{137}Sb is based on the present work. The $Q_{\beta-}$ and neutron separation energies (S_n, S_{2n}) are taken from Ref. [23]. Level information such as excitation energies, spin-parities, β-branching ratios, and log ft values are represented. Excited states newly established in the present work are represented in red.

intensities would be expected.

The 62-keV transition is predominant in the low-energy region of the spectrum shown in Fig. 1(a). It is observed in prompt coincidence with several other transitions as shown in Fig. 2(a). Since the energy of this transition is low, the internal electron conversion effect has to be considered. This transition might be an $M1$ or an $E2$ transition because the 62-keV level is a candidate of $5/2^-$ or $3/2^-$, and the internal conversion coefficients are $\alpha_{M1} = 2.69(14)$ and $\alpha_{E2} = 9.4(6)$, respectively. Based on these values, $E2$ multipolarity can be ruled out since otherwise the absolute β feeding of the 62-keV level would become enormous. Consequently, a spin-parity of $(5/2^-)$ is proposed for this state in ^{137}Te which decays

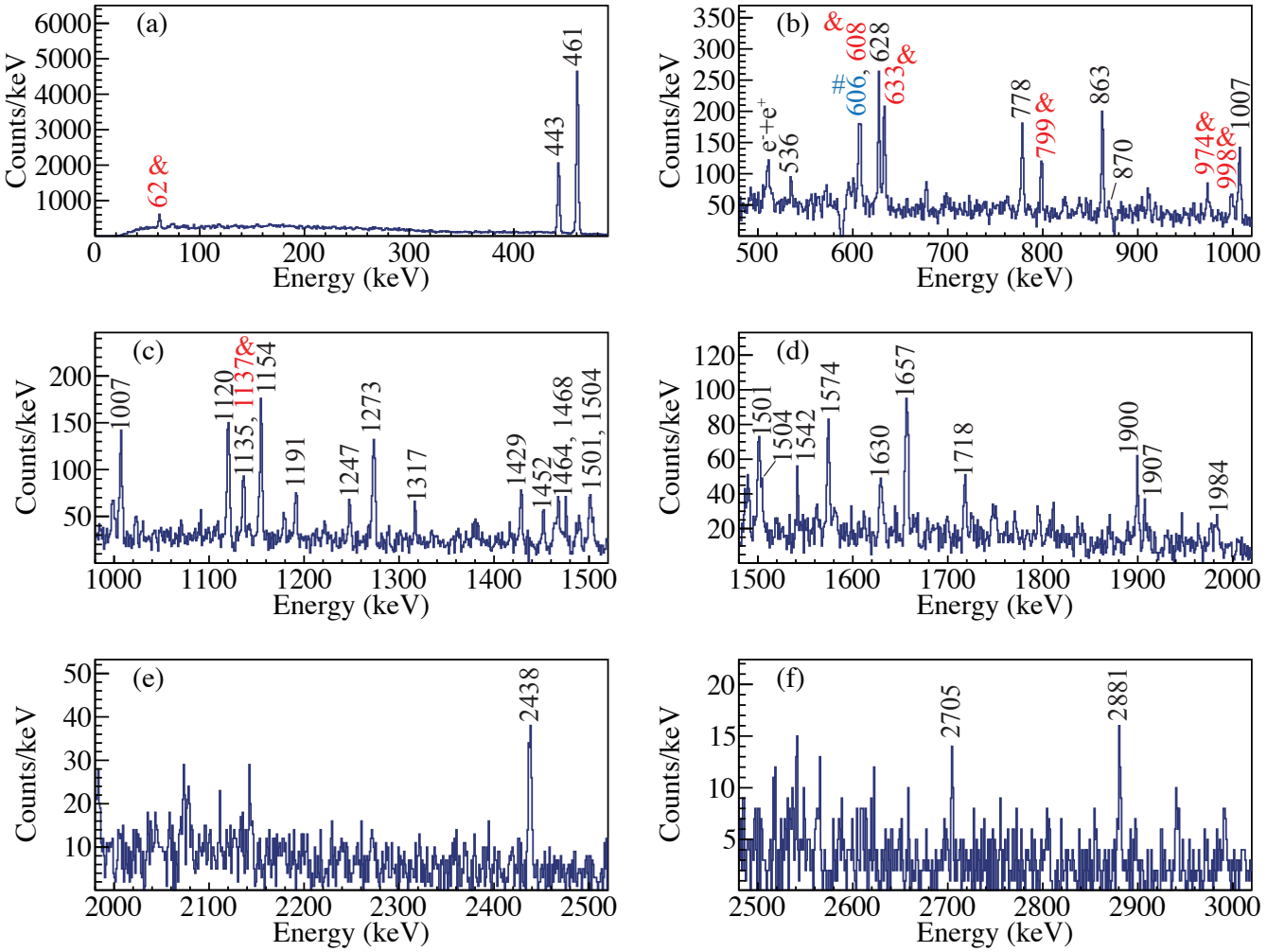

FIG. 4. Background-subtracted β-delayed γ-ray singles spectrum of ^{138}Sb. Black numbers represent the energies of the γ-ray transitions following β decay while red (blue) numbers marked by & (#) indicate transitions following the β-delayed emission of one (two) neutron(s).

by an $M1$ transition to the $(7/2^-)$ ground state.

As shown in Fig. 2(a), the 571-keV transition is coincident with the 62-keV transition. The γ-ray energy sum produces 633 keV, which corresponds to one of the predominant peaks in Fig. 1(a). Thus, a new excited state with an energy of 633 keV is established which decays to the low-lying $(5/2^-)$ state at 62 keV as well as to the $(7/2^-)$ ground state. Taking into account the relative γ-ray intensities, this state is a strong candidate for a $(9/2^-)$ state. Moreover, the systematics of the excitation energies of $9/2^-$ states in neighboring nuclei supports this assignment. A more detailed discussion will be presented in Section IV.1.

Additional excited states with energies of 799, 974, 998, and 1137 keV are proposed. These states are populated with log ft values corresponding to first-forbidden transitions [24–27] and therefore are expected to have spin-parities in the range from $(3/2^-)$ to $(11/2^-)$. However, the spin-parities for these states can be further limited by $(5/2^-, 7/2^-, 9/2^-)$ if we consider only unique decays. Specifically, among them, the 799- and 974-keV levels could be more strictly assigned as $(9/2^-)$ based on the systematic approach and shell-model calculation results. Details will be discussed later in this paper. Finally, a state at an excitation energy of 1726 keV was established in the current work based on γ-γ coincidence relations and γ-ray energy sums. This level has a log ft value of 5.6(1), in agreement with either a fast first-forbidden or an allowed transition. While it is thus not possible to firmly assign a parity, the observation of three decay branches to states with spins of $(5/2^-)$, $(7/2^-)$, and $(9/2^-)$, respectively, suggests a spin of (7/2) for the new 1726-keV level.

In Fig. 3, lower limits for the β-delayed 2n, 1n, and 0n emission probabilities to ^{135,136,137}Te can be estimated by the sum of the β-branching ratios, I_{β^-}. Unfortunately, only lower limits could be determined since these values are estimated based on the γ-ray intensities and direct feeding to the ground states is thus not accounted for. Note that such feeding must exist since the sum of the β

TABLE I. Transition energies (E_γ), relative γ-ray intensities (I_γ), and placements of γ rays emitted following the β decay of ^{137}Sb. The number in the parentheses is an error in the last digit. Systematic uncertainties of 0.25 keV and 5% for E_γ and I_γ, respectively, are included. The relative intensity should be multiplied by a factor of 0.23(2) to obtain the absolute intensity per 100 decays. This factor is deduced by the ratio between the 606.2-keV γ-ray events and the total β-ray events after subtracting the backgrounds.

E_γ (keV)	I_γ (rel)[a]	$E_{\mathrm{level},i}$ (keV)	$E_{\mathrm{level},f}$ (keV)
61.8(3)	93(26)[b]	61.8	0
352.4(3)[c]	14.0(39)	1382.3	1029.9
423.7(3)[c]	45.9(71)	1029.9	606.2
571.1(4)	12.2(68)	633.1	61.8
606.2(4)[c]	100(9)	606.2	0
608.1(4)	31.3(64)	608.1	0
633.2(3)	52.1(80)	633.1	0
752.2(5)	7.8(22)	1725.6	974.0
799.3(3)	17.1(42)	799.3	0
859.3(4)[c]	9.2(36)	1889.2	1029.9
912.4(4)	7.8(34)	974.0	61.8
961.1(4)[c]	10.2(31)	1567.3	606.2
973.8(3)	18.7(43)	974.0	0
998.3(4)	9.7(35)	998.3	0
1091.9(3)	20.5(44)	1725.6	633.1
1136.6(4)	13.1(57)	1136.6	0
1179.2(3)[c]	16.2(44)	1179.2	0
1663.8(4)	10.3(37)	1725.6	61.8
1725.7(3)	28.1(65)	1725.6	0

[a] The relative γ-ray intensity, I_γ, is normalized to the intensity of the 606.2-keV transition.
[b] I_γ reported here is the total γ-ray and internal conversion electron intensities, calculated assuming $M1$ multipolarity.
[c] γ-ray transitions observed following β-delayed neutron emission.

feeding to excited states does not yield 100%. In the β decay of ^{135}Sb [22], the ground state of ^{135}Te is strongly populated via the spin-flip first-forbidden transition from $(7/2^+)$ to $(7/2^-)$. Consequently, the branching ratio of the ground state of ^{137}Te probably accounts for most of the missing intensity of 13.3(85)%. Finally, we note that the γ-ray intensities quoted in Fig. 3 may be influenced by the Pandemonium effect [28], which leads to apparently stronger populations of the low-lying levels.

III.2. Beta decay of ^{138}Sb

The structure of ^{138}Te has already been investigated in several experiments prior to this work [12, 29, 30]. In the first measurement using spontaneous fission of ^{248}Cm, the yrast-band structure was established [29], although the order of the first two transitions, and therefore the energies of the 2_1^+ and 4_1^+ states, was wrongly assigned. A first β-decay scheme of ^{138}Sb, established on the basis of the data from the Te campaign (see section II.), was previously reported in Ref. [12]. The prominent difference between the relative intensities of the 461- ($2^+\rightarrow0^+$) and 443-keV ($4^+\rightarrow2^+$) transitions allowed to correct the 2_1^+ and 4_1^+ level energies [12]. In addition, a recent measurement, again using spontaneous fission of ^{248}Cm, allowed to further extend the high-spin level scheme and the collective-band structure, particularly related to the γ-soft vibration [30]. In the present work, we extend the known excitation scheme by several new non-yrast states, populated in the β decay of ^{138}Sb.

The background-subtracted β-delayed γ-ray singles spectrum of ^{138}Sb is represented in Fig. 4. Since ^{138}Sb has a shorter half-life as compared to ^{137}Sb, the prompt

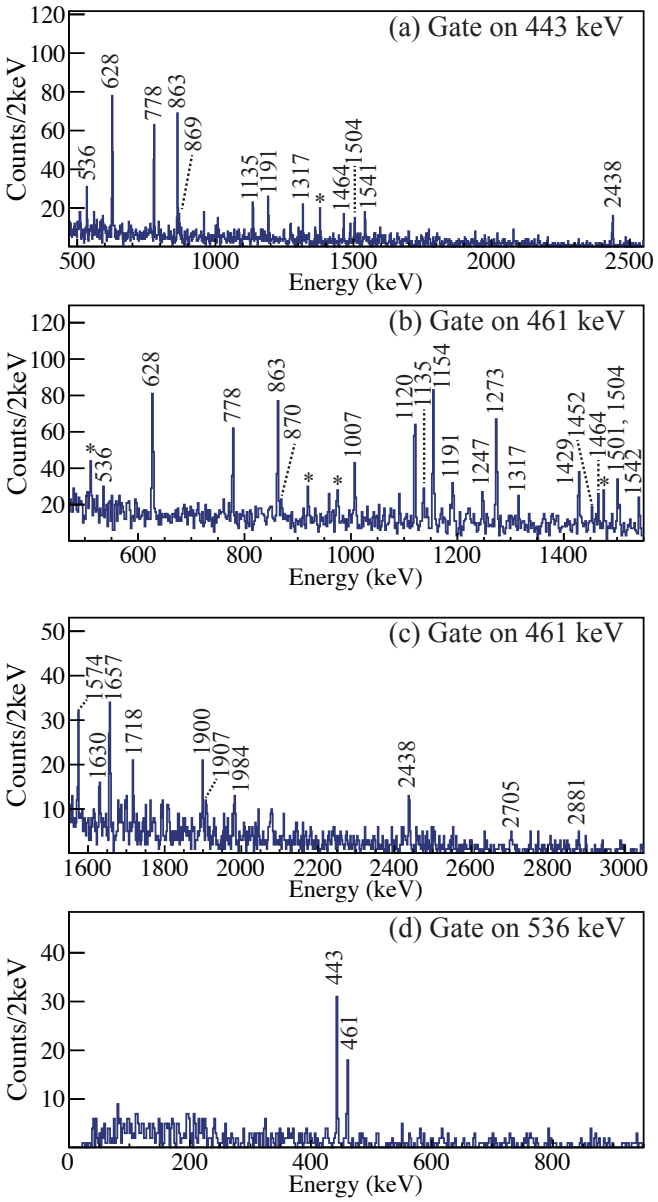

FIG. 5. γ-γ coincidence spectra with gate on (a) the 443-keV, (b),(c) the 461-keV, and (d) the 536-keV transition. Coincident transitions are indicated with their energies and contaminants are labeled with asterisks (*).

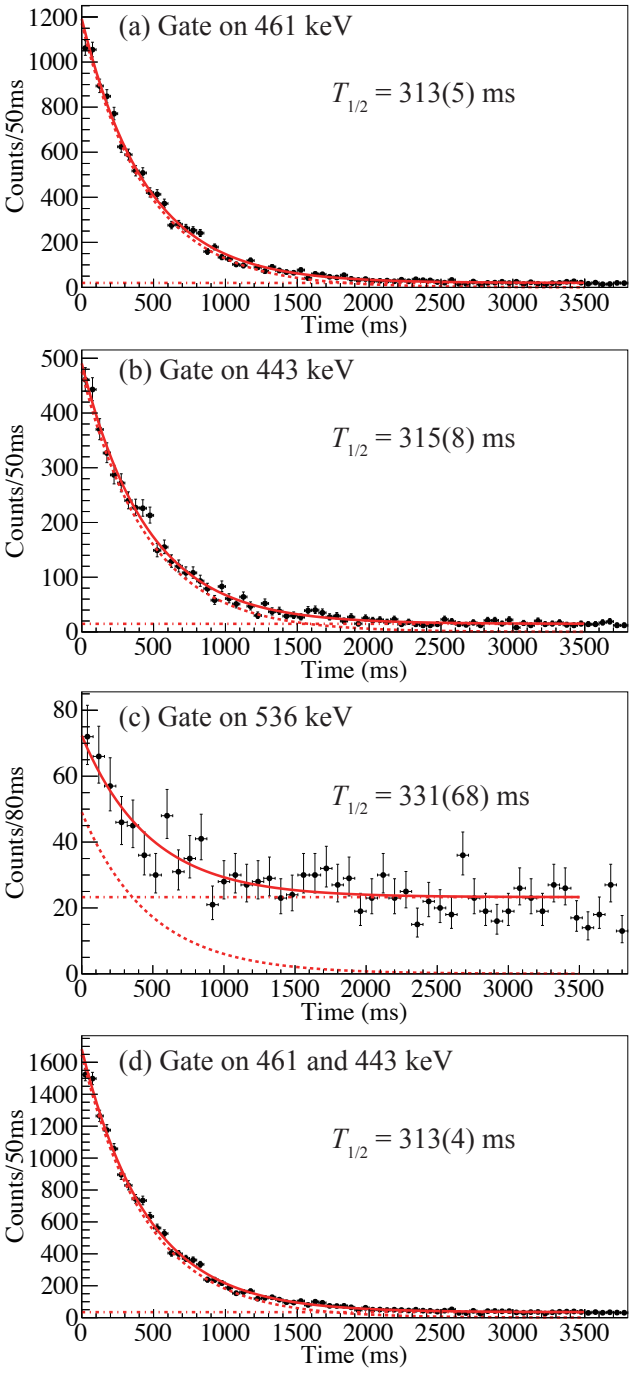

FIG. 6. Half-life measurements of the ground state of ^{138}Sb. Red solid lines indicate the fit results with a single-component exponential decay curve (red-dashed lines) and a constant background (red dashed-dotted lines).

and delayed time gates were set to the ranges $0-1000$ ms and $2500-3500$ ms, respectively. As in the case of ^{137}Sb, only those events were considered in which the ion and the β ray were detected in the same pixel of WAS3ABi. Table II summarizes the γ transitions observed following the β decay of ^{138}Sb. γ-γ coincidence spectra with gates on the 443-, 461-, and 536-keV transitions are shown in Fig. 5. As can be seen in that figure, the 863-keV transition is observed in coincidence with both the 443- and 461-keV γ rays. This result contradicts the previous assignment of a 2_2^+ state with an excitation energy of 1323 keV [12]. In Fig. 4(b), a weak line is visible at an energy of 536 keV, i.e. the energy of the $6^+\rightarrow4^+$ transition in ^{138}Te [15, 29, 30]. The observation of a 536-keV γ ray also in coincidence with the 461- and 443-keV transitions, see Figs. 5(a),(b), and (d), confirms that this γ ray does not belong to a contamination or one of the neutron emission channels but indeed stems from the decay of the 6^+ state. The direct population of this state in the decay of the (3^-) ground state of ^{138}Sb is not expected since the maximum spin difference for a first-forbidden transition is $\Delta J = 2$. There are three possible explanations for the observation of the 536-keV γ ray in the present data. The first is, that the ^{138}Sb ground state spin is actually higher than (3^-), although the β feeding and the log ft values measured in this work do not seem to support this hypothesis. The second possible explanation is the existence of a β-decaying isomer in ^{138}Sb, which has a higher spin than the (3^-) ground state. In order to search for experimental evidence for this scenario, the decay curves obtained in coincidence with the 461, 443, and 536-keV transitions are shown in Figs. 6. The half-life values obtained from a fit of these curves are in agreement and therefore do not provide any evidence for the existence of more than one β-decaying state in ^{138}Sb. However, due to the large uncertainty of the half-life determined in coincidence with the 536-keV transition this option cannot completely be excluded. An alternative method to detect multiple β-decaying states is to compare the β feeding to the 2_1^+ and 4_1^+ states in two different β-decaying cascades, namely ^{138}Sb$\rightarrow^{138}$Te and ^{138}Sn$\rightarrow^{138}$Sb$\rightarrow^{138}$Te. However, this method can unfortunately not be applied in the present case due to the low statistics obtained for the ^{138}Sn decay in the present experiment [31]. As shown in Fig. 6(d), a half-life of $T_{1/2}$=313(4) ms is determined from the sum of the gates on the $4^+\rightarrow2^+$ and $2^+\rightarrow0^+$ transition. This value is smaller as compared to the previously published measurements, 346(19) ms [12] and 350(15) ms [21], but similar to the value $T_{1/2}$=326(8) ms reported recently in Ref. [3]. Finally, the third explanation for the observation of the 536-keV transition is the population of the 6^+ state via γ transitions from higher-lying states rather than direct β feeding. This explanation has already been put forward in a similar case, namely the β decay of the 1^- ground state of ^{136}Sb [32]. In that case, a population of the 4^+ state in ^{136}Te was detected by the observation of a weak $4^+\rightarrow2^+$ transition, in complete analogy to the present situation. On the basis of the currently available experimental information we tend to adopt this explanation also in the present case.

The decay scheme of ^{138}Sb, which was considerably extended in the present work, is illustrated in Fig. 7. The assignment of spins and parities to the levels of ^{138}Te was carried out based on the log ft values [24–27]. However, it is not possible to propose unique spin-parity values since most of the β decays in this region are governed by

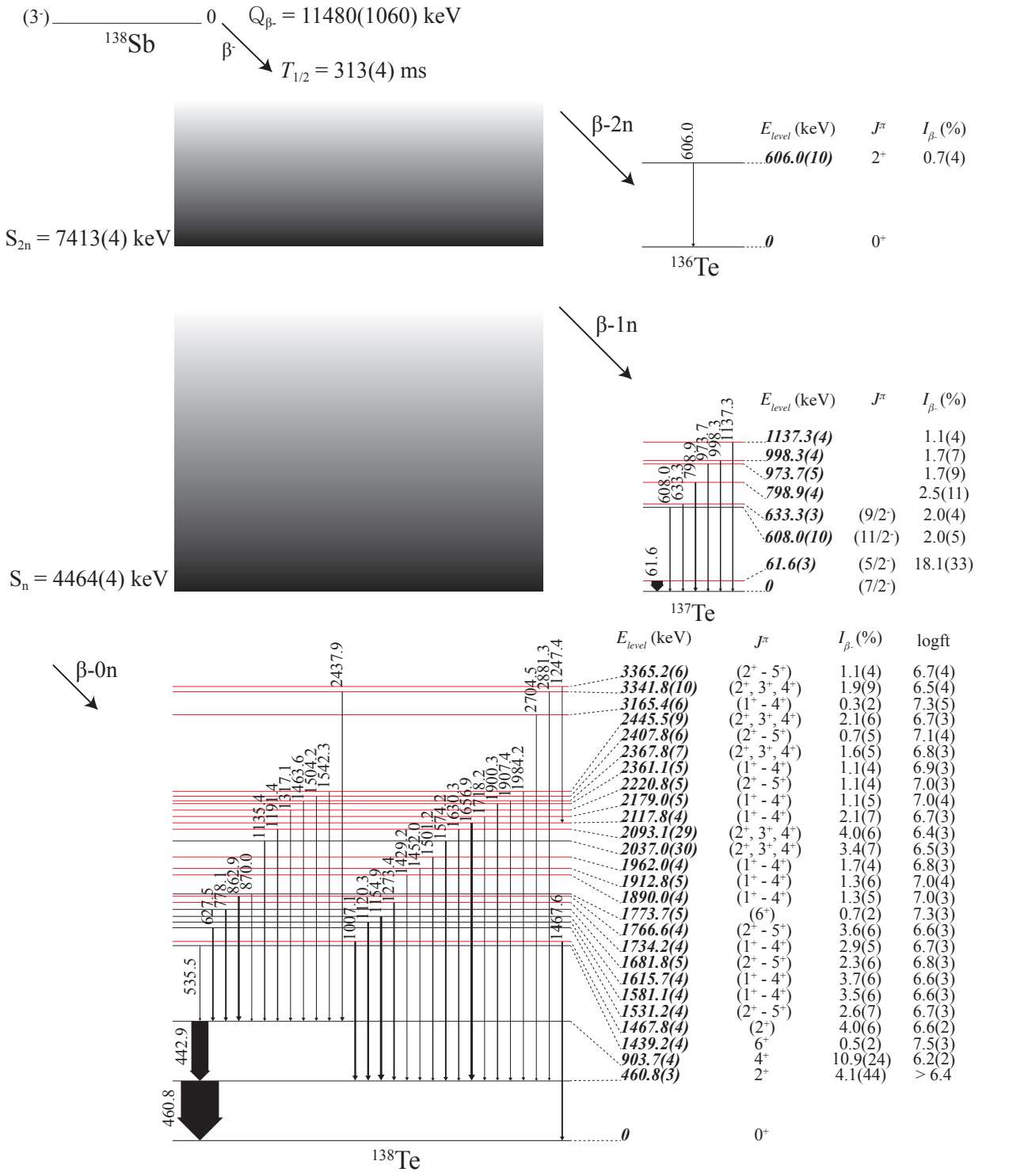

FIG. 7. β-decay scheme of ^{138}Sb. The half-life of the ground state of ^{138}Sb is based on the present work. The $Q_{\beta-}$ and neutron separation energies (S_n, S_{2n}) are taken from Ref. [23]. Level information such as excitation energies, proposed spin-parities, β-branching ratios, and log ft values are represented. Newly assigned excited states from the present work are represented in red.

first-forbidden transitions. Nevertheless, for several levels spin values or ranges can be proposed. For instance, the level located at 1774 keV was assigned as (6^+) in the spontaneous fission experiment [30]. Moreover, the 1468-keV level is proposed to be the (2_2^+) state due to its decay paths to the ground state and the 2_1^+ level. On the other hand, three groups of levels could be restricted in their spin-parities based on the γ-decay patterns. One of them

has two γ-decay paths, levels do not only decay to the 2_1^+ state, but also to the 4_1^+ state. Therefore, these levels may have a spin-parity of $(2^+, 3^+, 4^+)$. The other group has the spin range from 1 to 4, and the levels belonging to this group have a γ transition to the 2_1^+ state. The remaining levels which populate 4_1^+, are left with spin-parities in the range 2^+ to 5^+. However, last two groups might be more strictly limited in their spin-parities to $(2^+, 3^+, 4^+)$ if only unique decays are considered.

IV. DISCUSSION

In order to quantitatively understand the observed level structures of ^{137}Te and ^{138}Te, large-scale shell-model calculations with two different effective interactions were performed. The shell-model spaces of both calculations are based on the same valence region outside the doubly-magic ^{132}Sn core with $Z = 50$ and $N = 82$: the $0g_{7/2}$, $1d_{5/2}$, $1d_{3/2}$, $2s_{1/2}$, and $0h_{11/2}$ proton orbitals and the $1f_{7/2}$, $0h_{9/2}$, $2p_{3/2}$, $1f_{5/2}$, $2p_{1/2}$, and $0i_{13/2}$ neutron orbitals. Both interactions were derived within the framework of many-body perturbation theory starting from free nuclear potentials renormalized using the low-momentum potential approach [34]. In particular, the $\hat{Q}$-box-folded-plus-folded-diagram method [35, 36] has been employed by including in the perturbative diagrammatic expansion of the $\hat{Q}$ box one- and two-body diagrams up to second order in the interaction. The first interaction, which in the following is called Napoli, is based on the CD-Bonn NN potential [37], and has been adopted in several previous studies of neutron-rich nuclei beyond ^{132}Sn [38]. Particularly, it is shown that it reproduces very well the observed level scheme of ^{134}Sb, with one valence proton and one valence neutron, and the low-lying $5/2^+$ state in ^{135}Sb [39, 40]. The second employed interaction, named N3LOP, is derived from the realistic N3LO Chiral effective field theory potentials [41]. Some monopole and multipole adjustments are included in order to reproduce the isomeric transitions in the Sn isotopes with $N > 82$ [14, 42] and the single-particle energies of $N = 82, 83$ isotones. The N3LOP interaction has been employed to describe the spectroscopy and the overall feature of collectivity in isotones with $N = 84-88$ beyond doubly-magic ^{132}Sn [43–46], showing nice agreement with the data. The present Napoli and N3LOP calculations are performed using the Antoine shell-model code [47, 48].

IV.1. Neutron levels and seniority-3 configurations in ^{137}Te

For neutron-rich Te isotopes beyond $N = 83$, the single-particle states are not very well established so far [15]. In the case of ^{135}Te, excited states with spins of $7/2^-$, $3/2^-$, $1/2^-$, $5/2^-$, and $9/2^-$ are assigned [22]. From shell-model calculations [49], it turns out that the first $7/2^-$, $3/2^-$, and $1/2^-$ states have the largest spectroscopic factors for adding a neutron in the corresponding single-particle orbital to the ^{134}Te ground state. The second $9/2^-$ state, which can be associated with the experimental 1.38 MeV state with uncertain spin-parity assignment, carries the largest fraction of the single-particle strength. As for the $\nu 1f_{5/2}$ orbital, no significant strength is predicted to be carried by the low-lying $5/2^-$ states. Moreover, it should be emphasized that when more valence neutrons occupy the $1f_{7/2}$ orbital, as in the $N = 85, 87$ isotones, low-lying $(7/2^-)$, $(5/2^-)$, and $(3/2^-)$ states close to the ground states are formed that are not observed in the $N = 83$ isotonic chain [15]. In particular, the yrast excitations in ^{137}Te are supposed to be formed by the three valence neutrons in the $1f_{7/2}$ and $0h_{9/2}$ orbitals coupled to core vibrations [20]. On the other hand, the properties of the ^{139}Te nucleus indicate that, at neutron number $N = 87$, a transition between spherical and prolate shapes takes place along the Te chain of isotopes [50]. Consequently, it is crucial to investigate the low-lying levels in odd-A Te isotopes to understand the nuclear structure evolution, specifically the neutron one, beyond ^{132}Sn.

Figure 8 shows the systematics of excitation energy differences along the $N = 85$ isotones, in which the newly observed levels from this work are included. The reported excitation energies are referred to the low-lying $7/2^-$ states. Particularly, one may notice that the $11/2^-$ levels correlate with the 2_1^+ levels in the neighboring $N = 84$ nuclei, which are also displayed in the figure. This result strongly supports that the observed $11/2^-$ state in ^{137}Te is formed by a neutron coupled to the 2_1^+ state of ^{136}Te, namely $(\nu 1f_{7/2} \otimes 2^+)_{11/2^-}$. Moreover, we see that low-lying $(5/2^-)$ and $(3/2^-)$ states near the $(7/2_1^-)$ states are present in the spectra of the $N = 85$ isotones for $Z \geq 54$. The systematic trend of the $5/2^-$ states reasonably supports our $5/2^-$ assignment for the first excited state of ^{137}Te. However, a $3/2^-$ state is not identified in the present work. It is probably located close to the

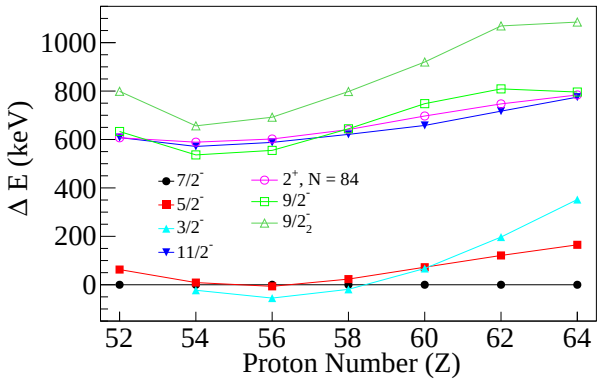

FIG. 8. Excitation energy differences of excited states in the $N = 85$ isotones relative to the $7/2_1^-$ levels. Data for ^{137}Te are taken from this work, and all others are taken from Ref. [15]. For $9/2_2^-$ states of ^{143}Ce ($Z = 58$) and ^{149}Gd ($Z = 64$), the levels at 817 keV and 1085 keV without explicit spin-parity assignment are included, based on systematics.

62-keV $5/2^-$ state.

As for the 633-keV level in ^{137}Te, we propose a spin-parity value of $J^\pi = 9/2^-$ as suggested by the behavior of the first $9/2^-$ states in the heavier $N = 85$ isotones. On the other hand, the newly established state at 799 keV is associated with the second $9/2^-$ state. In fact, with this assignment, the energy difference between the $(9/2_1^-)$ and $(9/2_2^-)$ states is consistent with those observed in the other isotones with $Z \geq 54$ as shown in Fig. 8.

The shell-model results obtained with the Napoli and N3LOP interactions are reported and compared with the experimental data in Fig. 9. Moreover, in order to obtain a better insight into the structure of ^{137}Te, the percentage contributions of the $\nu(1f_{7/2})^3$ configuration from both interactions are summarized in Table. III, together with some spectroscopic factors involving the addition of one neutron to the ground and first 2^+ states of ^{136}Te, indicated, respectively, as $C^2S(0^+)$ and $C^2S(2^+)$. First of all, both calculations nicely predict a $7/2^-$ ground state, together with the low-lying $5/2^-$ excited state whose energy is in good agreement with the experimental value. It is worth noting, however, that the Napoli interaction overestimates the $7/2^- - 5/2^-$ gap, which, in contrast, is slightly too small when using the N3LOP interaction. A similar difference between the two calculations is found for the unknown yrast $3/2^-$ state (see Fig. 9) and for the yrast $5/2^+$ and $3/2^+$ states of ^{137}Sb [31].

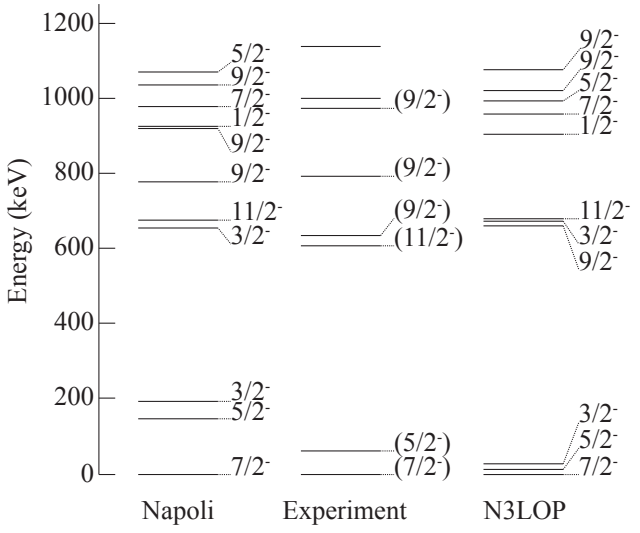

FIG. 9. Comparison between the experimentally established negative-parity states of ^{137}Te (middle) and theoretical predictions. The Napoli (left) and N3LOP (right) interactions are employed in the large-scale shell-model calculations.

It is of great importance to understand the origins of these low-lying $7/2^-$, $5/2^-$, and $3/2^-$ levels since these levels close to the ground state are not observed in the $N = 83$ isotones with a single neutron above the $N = 82$ shell gap. Based on both shell-model calculations, the $7/2^-$ ground state can be identified as a single-neutron state. As reported in Table III, both calculations produce large spectroscopic factors coupling a neutron in the $1f_{7/2}$ orbital to the 0_1^+ state of ^{136}Te. This ground state is also dominated by the $\nu(1f_{7/2})^3$ configuration which is contributing with 61% and 54%, respectively in the Napoli and N3LOP calculations. Moreover, the neutron occupancies of the $1f_{7/2}$ orbital are 2.4 (Napoli) and 2.3 (N3LOP) over 3. On the other hand, the yrast $5/2^-$ and $3/2^-$ states show essentially a seniority-3 ($\nu = 3$) nature. For these states, a large contribution arises from the $\nu(1f_{7/2})^3$ configuration: 53% ($5/2^-$) and 44% ($3/2^-$) from Napoli; 46% ($5/2^-$) and 37% ($3/2^-$) from N3LOP. Furthermore, large spectroscopic factors are found for the addition of a neutron in the $1f_{7/2}$ orbital to the 2_1^+ state of ^{136}Te (see the $C^2S(2^+)$ values in Table. III).

The first $9/2^-$ state predicted by both calculations is dominated by the $\nu(1f_{7/2})^2(2p_{3/2})^1$ and $\nu(1f_{7/2})^3$ configurations. Moreover, this state mainly originates from the coupling between a neutron in the $1f_{7/2}$ orbital and the 2_1^+ state of ^{136}Te, as shown by the corresponding spectroscopic factors of 0.38 (Napoli) and 0.41 (N3LOP), as . The observed 633-keV level might be a good candidate for this state, predicted at 660 keV by N3LOP, and at a slightly higher energy of 777 keV by Napoli. The second $9/2^-$ state at 920 keV from Napoli and the third $9/2^-$ state at 1078 keV from N3LOP also show the same $\nu = 3$ nature, but they are both dominated by only the $\nu(1f_{7/2})^3$ configuration. On the other hand, the third $9/2^-$ state at 1035 keV from Napoli and the second $9/2^-$ state at 1023 keV from N3LOP are predicted to be of single-neutron nature, $\nu 0h_{9/2} \otimes 0^+$, based on the calculated spectroscopic factors (see Table III) and the $\nu 0h_{9/2}$ occupation which is 0.86 (Napoli) and 0.74 (N3LOP).

From the experiment, the observed level at 799 keV might be a $9/2^-$ state, as described previously in terms of the systematic approach. On the other hand, the strong candidate for the third $9/2^-$ state from the present work is the level at 974 keV, since it shows the similar decay pattern as the 633-keV level. Thus, we can suppose that this 974-keV level is governed by the $\nu 1f_{7/2} \otimes 2^+$ configuration, corresponding to the second and third $9/2^-$ states predicted by the Napoli and N3LOP interactions, respectively. The 799-keV state may therefore be recognized as a single-neutron state and associated to the predicted 1035 and 1023 keV levels. It is worth noting, however, that its excitation energy is overestimated by about 200 keV in the calculations, which may lead to the conclusion that the ^{137}Te nucleus adopts a more deformed shape than expected. This statement is also supported by the predicted $11/2^-$ level energies, which are also slightly overestimated by both calculations. This result highly recommends direct reaction experiments that could confirm these findings providing precise spectroscopic factors of the excited states.

A similar scenario is noticed for the $3/2^-$ states. As discussed above, the yrast $3/2^-$ state is of $\nu = 3$ seniority nature, while it is the second one that carries the largest fraction of single-neutron strength. For this single-neutron nature $3/2_2^-$ state, the Napoli and N3LOP interactions predict excitation energies of 655 and 673 keV, respectively. The $1/2_1^-$ state is also expected to be

formed by a neutron in the $2p_{1/2}$ orbital coupled to the ^{136}Te ground state. At this point, it could be speculated that the sudden decrease of the energies of the first $3/2^-$ and $9/2^-$ states from ^{135}Te to ^{137}Te is influenced by the drastic decrease of the yrast 2^+ state energy between ^{134}Te and ^{136}Te, whose nature changes from proton to neutron excitation. In contrast, the $1/2^-_1$ state energy remains constant, keeping its single-particle nature. However, unfortunately no experimental information about these levels could be obtained from the present data.

The $7/2^-_2$ level is predicted to be formed by significant contributions from the $\nu(1f_{7/2})^2(2p_{3/2})^1$ and $\nu(1f_{7/2})^3$ neutron configurations, while a broadly mixed configuration involving all the neutron $1f_{7/2}$, $0h_{9/2}$, $1f_{5/2}$, and $2p_{3/2}$ orbitals is expected for the $5/2^-_2$ state. There is no clear evidence to assign these states from the experiment, but levels at 997 and 1137 keV might be candidates.

The $11/2^-$ levels from both calculations show, despite a small overestimation, good agreement with the observed level at 608 keV. This level is expected, as discussed previously, to arise from the coupling between a neutron in the $1f_{7/2}$ orbital and the 2^+_1 state of ^{136}Te. Theoretical predictions show that this $11/2^-$ level is strongly dominated by the $\nu(1f_{7/2})^3$ configuration with 59% and 48%, respectively deduced by the Napoli and N3LOP interactions. On the other hand, the collectivity in terms of the energy ratio parameter $E(15/2^-)/E(11/2^-) = 1.88$ [20] shows a transitional phase from ^{136}Te ($R_{4/2} = E(4^+)/E(2^+) = 1.69$) to ^{138}Te ($R_{4/2} = 1.96$).

With respect to the proposed (7/2) level at an excitation energy of 1726 keV, populated with a log ft value of 5.6(1), the interpretation is unfortunately not obvious. In most of the β decays of $Z = 50$, 51 nuclei studied so far only first-forbidden transitions to excited states below the neutron separation energy in the daughter nuclei were observed. Examples are the decays of ^{134,135}Sn and ^{135,136}Sb [22, 32, 51, 52]. The only relevant Gamow-Teller (GT) decay in this region is the $\nu 0h_{9/2}\rightarrow\pi 0h_{11/2}$ transition, which is hindered by the small occupancy of the $\nu 0h_{9/2}$ orbital in the ground states of these nuclei. Recently, the population of a state at 2641 keV in ^{136}Sb in the β decay of ^{136}Sn with log ft=5.2(2) was proposed to correspond to such an allowed $0^+\rightarrow(1^+)$ transition [31]. In that case, 1^+ states with the proper configuration were identified in the shell-model calculations 0.64/0.86 MeV too high in energy. For ^{137}Te, the calculations performed with the Napoli and N3LOP interactions predict the first positive-parity states at 2086 keV and 1847 keV, respectively, but these states are $13/2^+$ states. The lowest $7/2^+$ states are expected to be located at 2814 keV (Napoli) and 2765 keV (N3LOP), i.e. about 1 MeV above the experimentally identified (7/2) level. However, these levels do not have the configuration required for a state which is populated via the allowed $\nu 0h_{9/2}\rightarrow\pi 0h_{11/2}$ decay. In contrast to the case of ^{136}Sb, for ^{137}Te no matching calculated $7/2^+$ state is found around 1.7 MeV. The only possible explanation for the observation of a positive-parity state would be the coupling of the odd $1f_{7/2}$ neutron in ^{137}Te to the octupole 3^- state in ^{136}Te. Although the energy of the latter is unknown, the systematics of 3^- states in the N=84 isotones suggests a much higher excitation energy for a positive-parity state of this origin in ^{137}Te. Given the log ft value of 5.6(1), the 1726-keV state could as well be a $(7/2^-)$ state populated via a first-forbidden transition. We note that in neighboring nuclei, several decays via the $\nu 1f_{7/2}\rightarrow\pi 0g_{7/2}$ spin-flip transition have been observed with log ft values in the range 5.2-5.8 [22, 32, 51, 52]. The present shell-model calculations indeed predict several $7/2^-$ states in the energy region around 1.7 MeV.

IV.2. Nuclear structure of ^{138}Te

The collectivity of the $N = 86$ isotones has been investigated in detail in Refs. [30, 43–45], where the first evidence of the γ-vibrational band in ^{138}Te was discussed. On the other hand, the recent experimental result of Ref. [13] has suggested for ^{140}Te with $N = 88$ a typical vibrational character in terms of the energy ratio $R_{4/2} = 2.01$. Consequently, the Te isotopes beyond the neutron magic number $N = 82$ turn out to show a differ-

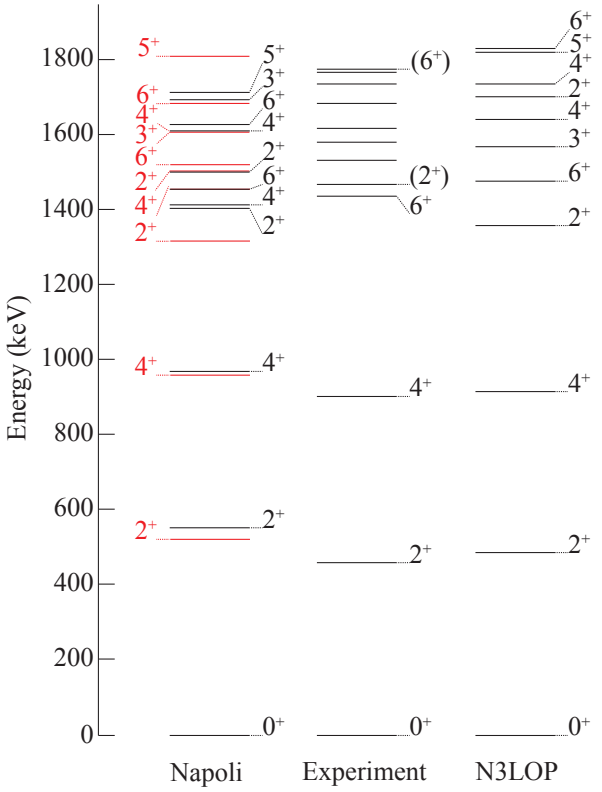

FIG. 10. Comparison between the experimentally established levels of ^{138}Te (middle) and theoretical predictions. The Napoli (left) and N3LOP (right) interactions are employed in the large-scale shell-model calculations. A modified version of the Napoli interaction is shown in red, see text for details.

ent nature in the structure evolution as compared to the neighboring Sn [14] and Xe [53] nuclides.

In the present work, new abundant non-yrast states have been observed with a very high level density as shown in Fig. 7. Even though a one-to-one correspondence between calculated and observed levels is not free of some ambiguity due to the experimental uncertainties in the spin assignment, the levels below 1800 keV can be reasonably well explained by theory. Figure 10 shows the experimental excitation energies together with the results from the Napoli and N3LOP calculations. As one may see, both theoretical predictions are in good agreement with the observed levels. Note that the spectrum in red in Fig. 10 is obtained by employing the modified Napoli interaction of Ref. [54] which will be discussed below. Additional information from the calculations, namely reduced transition rates $B(E2)$, spectroscopic quadrupole moments Q_s, and dimensionless nuclear magnetic moments g-factors are summarized in Table IV. All g-factor calculations are achieved using the effective spin and orbital g-factors $(g^s_\pi, g^l_\pi) = (3.250, 1.069)$ and $(g^s_\nu, g^l_\nu) = (-1.506, 0.019)$ for protons and neutrons, respectively [44, 46].

Most of all, it is worthwhile to discuss the yrast states of ^{138}Te. The predicted levels from N3LOP agree very well with the observed 2^+_1, 4^+_1, and 6^+_1 levels. Particularly, the $B(E2; 0^+ \rightarrow 2^+) = 0.316\ e^2\mathrm{b}^2$ value, calculated by using $e_p = 1.6\ e$ and $e_n = 0.6\ e$ as effective charges, indicates the evolution of collectivity in ^{138}Te. The recently measured $B(E2; 0^+ \rightarrow 2^+)$ values of ^{136}Te, which are 0.181(15) $e^2\mathrm{b}^2$ [7] and 0.191(26) $e^2\mathrm{b}^2$ [8], support this statement in terms of the nice agreement with systematics. The Napoli interaction, by using $e_p = 1.7\ e$ and $e_n = 0.7\ e$, also provides a consistent reduced transition rate of 0.318 $e^2\mathrm{b}^2$ although the 2^+_1 excitation energy is overestimated by 140 keV. Additionally, the two calculations predict very close $B(E2; 2^+ \rightarrow 4^+)$ values, which indicate a modest nuclear structure evolution as compared to the corresponding measured $B(E2)$ in ^{136}Te (0.060(9) $e^2\mathrm{b}^2$ [7] and 0.061(31) $e^2\mathrm{b}^2$ [8]). On the other hand, $B(E2; 4^+ \rightarrow 2^+)/B(E2; 2^+ \rightarrow 0^+) = 1.43$ (N3LOP) and 1.35 (Napoli) ratios give a strong evidence of the $K = 0$ quantum number for the yrast-band structure. Other features are already exposed in Refs. [44, 45], where the onset and the evolution of the quadrupole collectivity in $N = 86$, 88 isotones are evidenced. The N3LOP calculations have unveiled some triaxiality signature in ^{138}Te with a weak collective nature, distinguished by β =0.12 and γ =11° as deformation parameters [44]. This result strongly encourages a future measurement of the 2^+_1 and 4^+_1 lifetimes, which are expected to be around τ = 62 and 54 ps, respectively, based on the calculated $B(E2)$ values from the N3LOP and Napoli interactions, to confirm the nuclear structure evolution of Te isotopes in terms of quadrupole correlations.

On the contrary, it should be emphasized that different features are predicted by the N3LOP and Napoli interactions for the first 6^+ state. In fact, the absolute Q_s and $B(E2; 4^+_1 \rightarrow 6^+_1)$ values from Napoli are about a factor 2.3 and 1.8 smaller than those predicted by N3LOP (see Table IV). Moreover, from N3LOP this yrast 6^+ state is expected to be dominated by the proton $\pi(0g_{7/2})^1(1d_{5/2})^1$ configuration accounting for 31% of the calculated wave function, while the Napoli interaction provides only a 6% contribution of this proton configuration. In order to explain the differences between the two calculations, we have employed a modified version of the Napoli interaction. This new version, as discussed in Ref. [54], results from small changes of the $J = 2, 4, 6$ matrix elements of the $\nu(1f_{7/2})^2$ configuration, which were introduced to reproduce the isomeric transition $B(E2; 6^+_1 \rightarrow 4^+_1)$ in ^{136}Sn. For the same reason, a similar modification was previously included in the development of the N3LOP effective interaction [44]. The new Napoli interaction leads to $Q_s(6^+_1)$ and $B(E2; 4^+_1 \rightarrow 6^+_1)$ values very close to those obtained with the N3LOP interaction, and to an increase of the proton $\pi(0g_{7/2})^1(1d_{5/2})^1$ contribution from 6% to 29%.

In this context, it is very interesting to investigate the seniority nature of the yrast 4^+ and 6^+ states. In both calculations, using either the Napoli or the N3LOP interaction, the 4^+_1 state turns out to be governed by seniority admixtures. It is dominated by the ν=4 component (50%), while the ν=2 and 6 contributions range from 20 to 30%. On the contrary, different features are predicted by the two calculations for the 6^+_1 state. With the Napoli interaction, a large contribution, 52%, arises from the ν=2 component, while the ν=4 component only accounts for 15% of the wave function. However, when the modified Napoli interaction is employed, a significant seniority mixing is found for the 6^+_1 state: ν=2 (31%), ν=4 (32%), and ν=6 (37%), which is comparable to the N3LOP result, marked by ν=2 (21%), ν=4 (42%), and ν=6 (37%). It is worth noting that the seniority structure of the 6^+_1 state predicted by the modified Napoli interaction is similar to that of the 4^+_1 level, as it is also the case with the N3LOP interaction, which gives rise to larger reduced transition rates as compared to the result from the original Napoli interaction (see Table IV). Consequently, we can suggest that the seniority in ^{138}Te plays a different role as compared to the case of the neutron-rich Sn isotopes [14]. In the semi-magic Sn isotopes with $N > 82$, the major seniority difference between the yrast 4^+ (mixed seniority) and 6^+ ($\nu = 2$) states originates a long-lived 6^+ isomer. In contrast, for ^{138}Te, the mixture of the seniorities is almost the same for the 4^+_1 and 6^+_1 states, which might be the reason for the absence of such an isomeric 6^+_1 state.

We turn our attention now to the γ-band structure of ^{138}Te, which was previously discussed by employing the N3LOP interaction in Ref. [44]. Since the calculated $Q_s(2^+_2)$ has the same size as $Q_s(2^+_1)$ but an opposite sign, the 2^+_2 state from N3LOP could be interpreted as a γ-band head state. The fact that $Q_s(3^+_1)$ is predicted to be close to zero and the $B(E2; 2^+_2 \rightarrow 3^+_1)$ is rather large (see Table IV) also supports this statement. Moreover, sizable transition strengths between the 2^+_2 and 4^+_2 states, and the 3^+_1 and 5^+_1 states can be noticed in Table IV

from the N3LOP interaction. On this basis, the 2_2^+, 3_1^+, 4_2^+, and 5_1^+ levels from N3LOP shown in Fig. 10 can be considered as belonging to the same γ-band structure. In the case of the Napoli interaction, we could draw similar conclusions about the γ-band nature of the 2_2^+ and 3_1^+ states. Although the absolute Q_s values are smaller than those from N3LOP, they firmly represent analogous aspects. It is worth noting, however, that this is not the case for the 4_2^+ and 5_1^+ levels. We see, in fact, that very small $B(E2; 3_1^+ \rightarrow 5_1^+)$ and $B(E2; 2_2^+ \rightarrow 4_2^+)$ values are predicted by the Napoli interaction. In contrast, the modified Napoli interaction reproduces reduced transition rates which are more consistent with the N3LOP results, although it is worth noting that Q_s values for the 5_1^+ and 4_2^+ states still remain very different. Therefore, it can be concluded that the modification in matrix elements of Napoli generally leads to results for ^{138}Te consistent with those of N3LOP. Unfortunately, it is difficult to confirm that the observed levels from the present work are formed by the γ-soft vibration because no linking γ-ray transition is observed. In Ref. [30], however, the minimum spin state of the γ-vibrational band is proposed to be a 7^+ state and lower-spin members such as the 4_2^+, 5_1^+, and 6_2^+ levels are also not linked to each other. Thus, it can be suggested that the weak quadrupole correlation of ^{138}Te is insufficient to form a robust γ-band structure like that observed in the heavier isotones.

V. CONCLUSION

In the present work, the β decays of the ^{137,138}Sb isotopes studied in two different EURICA experiments performed at the RIBF of RIKEN are reported. From the experimental results with respect to the ^{137}Sb β decay, several important excited states such as the $(5/2^-)$ and $(9/2^-)$ levels could be established. The ^{137}Te nucleus turned out to form the seniority-3 configuration of $\nu 1f_{7/2}$ in the low-lying states. Moreover, different nature of the observed $9/2^-$ states could be explained by employing two independent shell-model calculations based on the Napoli and N3LOP interactions. In particular, the calculated spectroscopic factors from both interactions show the excellent agreement, and this theoretical result paves the way to the future direct reaction experiments of this isotope.

Regarding the β decay of ^{138}Sb, the observed levels in ^{138}Te are in general well described by the shell-model calculations. Based on the theoretical predictions, the ^{138}Te nucleus is expected to exhibit a weak quadrupole deformation with $\beta = 0.12$. It can be concluded that the ^{138}Te nucleus shows a modest nuclear structure evolution with a weak quadrupole correlation based on the overall features supported by theory.

ACKNOWLEDGMENTS

This work was carried out at the RIBF operated by RIKEN Nishina Center and CNS, University of Tokyo. We acknowledge the EUROBALL Owners Committee for the loan of germanium detectors and the PreSpec Collaboration for the readout electronics of the cluster detectors. Part of the WAS3ABi was supported by the Rare Isotope Science Project (RISP) of the Institute for Basic Science (IBS) funded by the Ministry of Science, ICT and Future Planning (MSIP) and National Research Foundation (NRF) of the Republic of Korea (Grant No. 2013M7A1A1075764). This research was supported by NRF of the Republic of Korea (Grant No. 2019R1A6A3A03031564 and 2018R1A5A1025563), IBS of the Republic of Korea (Grant No. IBS-R031-D1 and IBS-R031-Y1), the Spanish Ministerio de Economía y Competitividad (Grant No. FPA2017-84756-C4-2-P), and JSPS KAKENHI of Japan (Grant No. 25247045). The support from FR-JP LIA is also acknowledged. C. S. Lee acknowledges the support from NRF of the Republic of Korea (Grant No. 2017M2A2A6A02071071 and 2016R1D1A1A09917463). Zs. Vajta acknowledges the support from GINOP-2.3.3-15-2016-00034, K128947, and PD124717 projects. H. Naïdja is grateful to F. Nowacki for sharing Nathan code used in the seniority part.

[1] J. J. Cowan, F.-K. Thielemann, and J.W. Truran, Phys. Rep. **208**, 267 (1991).
[2] M. Mumpower, R. Suman, D. L. Fang, M. Beard, and A. Aprahama, J. Phys. G: Nucl. Part. Phys. **42**, 034027 (2015).
[3] J. Wu, S. Nishimura, P. Möller, M. R. Mumpower, R. Lozeva, C.-B. Moon, A. Odahara, H. Baba, F. Browne, R. Daido, P. Doornenbal, Y. F. Fang, M. Haroon, T. Isobe, H. S. Jung, G. Lorusso, B. Moon, Z. Patel, S. Rice, H. Sakurai, Y. Shimizu, L. Sinclair, P.-A. Söderström, T. Sumikama, H. Watanabe, Z. Y. Xu, A. Yagi, R. Yokoyama, D. S. Ahn, F. L. Garrote, J. M. Daugas, F. Didierjean, N. Fukuda, N. Inabe, T. Ishigaki, D. Kameda, I. Kojouharov, T. Komatsubara, T. Kubo, N. Kurz, K. Y. Kwon, S. Morimoto, D. Murai, H. Nishibata, H. Schaffner, T. M. Sprouse, H. Suzuki, H. Takeda, M. Tanaka, K. Tshoo, and Y. Wakabayashi, Phys. Rev. C **101**, 042801(R) (2020).
[4] K.-L. Kratz, B. Pfeiffer, and F.-K. Thielemann, Nucl. Phys. A **630**, 352c (1998).
[5] M. Arnould, S. Goriely, and K. Takahashi, Phys. Rep. **450**, 97 (2007).
[6] D. C. Radford, C. Baktash, J. R. Beene, B. Fuentes, A. Galindo-Uribarri, C. J. Gross, P. A. Hausladen, T. A. Lewis, P. E. Mueller, E. Padilla, D. Shapira, D. W. Stracener, C.-H. Yu, C. J. Barton, M. A. Caprio, L. Coraggio, A. Covello, A. Gargano, D. J. Hartley, and N. V. Zamfir, Phys. Rev. Lett. **88**, 222501 (2002).
[7] J. M. Allmond, A. E. Stuchbery, C. Baktash, A. Gargano, A. Galindo-Uribarri, D. C. Radford, C. R. Bingham, B. A. Brown, L. Coraggio, A. Covello, M. Danchev, C. J. Gross, P. A. Hausladen, N. Itaco, K. Lagergren, E.

Padilla-Rodal, J. Pavan, M. A. Riley, N. J. Stone, D. W. Stracener, R. L. Varner, and C.-H. Yu, Phys. Rev. Lett. **118**, 092503 (2017).

[8] V. Vaquero, A. Jungclaus, P. Doornenbal, K. Wimmer, A. M. Moro, K. Ogata, T. Furumoto, S. Chen, E. Nácher, E. Sahin, Y. Shiga, D. Steppenbeck, R. Taniuchi, Z. Y. Xu, T. Ando, H. Baba, F. L. Bello Garrote, S. Franchoo, K. Hadynska-Klek, A. Kusoglu, J. Liu, T. Lokotko, S. Momiyama, T. Motobayashi, S. Nagamine, N. Nakatsuka, M. Niikura, R. Orlandi, T. Y. Saito, H. Sakurai, P. A. Söderström, G. M. Tveten, Zs. Vajta, and M. Yalcinkaya, Phys. Rev. C **99**, 034306 (2019).

[9] J. Terasaki, J. Engel, W. Nazarewicz, and M. Stoitsov, Phys. Rev. C **66**, 054313 (2002).

[10] N. Shimizu, T. Otsuka, T. Mizusaki, and M. Honma, Phys. Rev. C **70**, 054313 (2004).

[11] D. Bianco, N. Lo Iudice, F. Andreozzi, A. Porrino, and F. Knapp, Phys. Rev. C **88**, 024303 (2013).

[12] P. Lee, C.-B. Moon, C. S. Lee, A. Odahara, R. Lozeva, A. Yagi, S. Nishimura, P. Doornenbal, G. Lorusso, P.-A. Söderström, T. Sumikama, H. Watanabe, T. Isobe, H. Baba, H. Sakurai, F. Browne, R. Daido, Y. Fang, H. Nishibata, Z. Patel, S. Rice, L. Sinclair, J. Wu, Z. Y. Xu, R. Yokoyama, T. Kubo, N. Inabe, H. Suzuki, N. Fukuda, D. Kameda, H. Takeda, D. S. Ahn, D. Murai, F. L. Bello Garrote, J. M. Daugas, F. Didierjean, E. Ideguchi, T. Ishigaki, H. S. Jung, T. Komatsubara, Y. K. Kwon, S. Morimoto, M. Niikura, I. Nishizuka, and K. Tshoo, Phys. Rev. C **92**, 044320 (2015).

[13] B. Moon, C.-B. Moon, P.-A. Söderström, A. Odahara, R. Lozeva, B. Hong, F. Browne, H. S. Jung, P. Lee, C. S. Lee, A. Yagi, C. Yuan, S. Nishimura, P. Doornenbal, G. Lorusso, T. Sumikama, H. Watanabe, I. Kojouharov, T. Isobe, H. Baba, H. Sakurai, R. Daido, Y. Fang, H. Nishibata, Z. Patel, S. Rice, L. Sinclair, J. Wu, Z. Y. Xu, R. Yokoyama, T. Kubo, N. Inabe, H. Suzuki, N. Fukuda, D. Kameda, H. Takeda, D. S. Ahn, Y. Shimizu, D. Murai, F. L. Bello Garrote, J. M. Daugas, F. Didierjean, E. Ideguchi, T. Ishigaki, S. Morimoto, M. Niikura, I. Nishizuka, T. Komatsubara, Y. K. Kwon, and K. Tshoo, Phys. Rev. C **95**, 044322 (2017).

[14] G. S. Simpson, G. Gey, A. Jungclaus, J. Taprogge, S. Nishimura, K. Sieja, P. Doornenbal, G. Lorusso, P.-A. Söderström, T. Sumikama, Z. Y. Xu, H. Baba, F. Browne, N. Fukuda, N. Inabe, T. Isobe, H. S. Jung, D. Kameda, G. D. Kim, Y.-K. Kim, I. Kojouharov, T. Kubo, N. Kurz, Y. K. Kwon, Z. Li, H. Sakurai, H. Schaffner, Y. Shimizu, H. Suzuki, H. Takeda, Z. Vajta, H. Watanabe, J. Wu, A. Yagi, K. Yoshinaga, S. Bönig, J.-M. Daugas, F. Drouet, R. Gernhäuser, S. Ilieva, T. Kröll, A. Montaner-Pizá, K. Moschner, D. Mücher, H. Naïdja, H. Nishibata, F. Nowacki, A. Odahara, R. Orlandi, K. Steiger, and A. Wendt, Phys. Rev. Lett. **113**, 132502 (2014).

[15] National Nuclear Data Center, Brookhaven National Laboratory, `http://www.nndc.bnl.gov`.

[16] T. Kubo, D. Kameda, H. Suzuki, N. Fukuda, H. Takeda, Y. Yanagisawa, M. Ohtake, K. Kusaka, K. Yoshida, N. Inabe, T. Ohnishi, A. Yoshida, K. Tanaka, and Y. Mizoi, Prog. Theor. Exp. Phys. 2012, 03C003 (2012).

[17] N. Fukuda, T. Kubo, T. Ohnishi, N. Inabe, H. Takeda, D. Kameda, and H. Suzuki, Nucl. Instrum. Methods Phys. Res., Sect. B **317**, 323 (2013).

[18] S. Nishimura, Prog. Theor. Exp. Phys. 2012, 03C006 (2012).

[19] P.-A. Söderström, S. Nishimura, P. Doornenbal, G. Lorusso, T. Sumikama, H. Watanabe, Z. Y. Xu, H. Baba, F. Browne, S. Go, G. Gey, T. Isobe, H.-S. Jung, G. D. Kim, Y.-K. Kim, I. Kojouharov, N. Kurz, Y. K. Kwon, Z. Li, K. Moschner, T. Nakao, H. Nishibata, M. Nishimura, A. Odahara, H. Sakurai, H. Schaffner, T. Shimoda, J. Taprogge, Zs. Vajta, V. Werner, J. Wu, A. Yagi, and K. Yoshinaga, Nucl. Instrum. Methods Phys. Res., Sect. B **317**, 649 (2013).

[20] W. Urban, A. Korgul, T. Rzaca-Urban, N. Schulz, M. Bentaleb, E. Lubkiewicz, J. L. Durell, M. J. Leddy, M. A. Jones, W. R. Phillips, A. G. Smith, B. J. Varley, I. Ahmad, and L. R. Morss, Phys. Rev. C **61**, 041301(R) (2000).

[21] O. Arndt, K.-L. Kratz, W. B. Walters, K. Farouqi, U. Köster, V. Fedosseev, S. Hennrich, C. J. Jost, A. Wöhr, A. A. Hecht, B. Pfeiffer, J. Shergur, and N. Hoteling, Phys. Rev. C **84**, 061307(R) (2011).

[22] P. Hoff, B. Ekström, and B. Fogelberg, Z. Phys. A - Atomic Nuclei **332**, 407 (1989).

[23] M. Wang, G. Audi, F. G. Kondev, W. J. Huang, S. Naimi, and X. Xu, Chin. Phys. C **41**, 030003 (2017).

[24] B. Singh, J. L. Rodriguez, S. S. M. Wong, and J. K. Tuli, Nuclear Data Sheets **84**, 487 (1998).

[25] H. Abele, M. A. Hoffmann, S. Baeβler, D. Dubbers, F. Glück, U. Müller, V. Nesvizhevsky, J. Reich, and O. Zimmer, Phys. Rev. Lett. **88**, 211801 (2002).

[26] B. Rubio, W. Gelletly, E. Nácher, A. Algora, J. L. Taín, A. Pérez, and L. Caballero , J. Phys. G, Nucl. Part. Phys. **31**, S1477 (2005).

[27] S. Raman, and N. B. Gove, Phys. Rev. C **7**, 5 (1973).

[28] J. Hardy, L. C. Carraz, B. Jonson, and P. G. Hansen, Phys. Lett. B **71**, 307 (1977).

[29] F. Hoellinger, B. J. P. Gall, N. Schulz, W. Urban, I. Ahmad, M. Bentaleb, J. L. Durell, M. A. Jones, M. Leddy, E. Lubkiewicz, L. R. Morss, W. R. Phillips, A. G. Smith, and B. J. Varley, Eur. Phys. J. A **6**, 375 (1999).

[30] W. Urban, K. Sieja, T. Rzaca-Urban, M. Czerwiński, H. Naïdja, F. Nowacki, A. G. Smith, and I. Ahmad, Phys. Rev. C **93**, 034326 (2016).

[31] A. Jungclaus, J. M. Keatings, G. S. Simpson, H. Naïdja, A. Gargano, S. Nishimura, P. Doornenbal, G. Gey, G. Lorusso, P.-A. Söderström, T. Sumikama, J. Taprogge, Z. Y. Xu, H. Baba, F. Browne, N. Fukuda, N. Inabe, T. Isobe, H. S. Jung, D. Kameda, G. D. Kim, Y.-K. Kim, I. Kojouharov, T. Kubo, N. Kurz, Y. K. Kwon, Z. Li, H. Sakurai, H. Schaffner, Y. Shimizu, H. Suzuki, H. Takeda, Z. Vajta, H. Watanabe, J. Wu, A. Yagi, K. Yoshinaga, S. Bönig, J.-M. Daugas, R. Gernhäuser, S. Ilieva, T. Kröll, A. Montaner-Piza, K. Moschner, D. Mücher, H. Nishibata, A. Odahara, R. Orlandi, M. Scheck, K. Steiger, and A. Wendt, Phys. Rev. C **102**, 034324 (2020).

[32] P. Hoff, J.P. Omtvedt, B. Fogelberg, H. Mach, and M. Hellström, Phys. Rev. C **56**, 2865 (1997).

[33] A. Tolosa-Delgado, J. Agramunt, J. L. Tain, A. Algora, C. Domingo-Pardo, A. I. Morales, B. Rubio, A. Tarifeno-Saldivia, F. Calvino, G. Cortes, N. T. Brewer, B. C. Rasco, K. P. Rykaczewski, D. W. Stracener, J. M. Allmond, R. Grzywacz, R. Yokoyama, M. Singh, T. King, M. Madurga, S. Nishimura, V. H. Phong, S. Go, J. Liu, K. Matsui, H. Sakurai, G. G. Kiss, T. Isobe, H. Baba, S. Kubono, N. Fukuda, D. S. Ahn, Y. Shimizu, T. Sumikama, H. Suzuki, H. Takeda, P. A. Söderström, M. Takechi, C. G. Bruno, T. Davinson, C. J. Griffin, O. Hall, D. Kahl, P. J. Woods, P. J. Coleman-Smith, M. Labiche,

I. Lazarus, P. Morrall, V. F. E. Pucknell, J. Simpson, S. L. Thomas, M. Prydderch, L. J. Harkness-Brennan, R. D. Page, I. Dillmann, R. Caballero-Folch, Y. Saito, A. Estrade, N. Nepal, F. Montes, G. Lorusso, J. Liang, S. Bae, J. Ha, and B. Moon, Nucl. Instrum. Methods Phys. Res., Sect. A **925**, 133 (2019).

[34] S. Bogner, T. T. S. Kuo, L. Coraggio, A. Covello, and N. Itaco, Phys. Rev. C **65**, 051301(R) (2002).

[35] M. Hjorth-Jensen, T. T. S. Kuo, and E. Osnes, Rev. Rep. **261**, 125 (1995).

[36] L. Coraggio, A. Covello, A. Gargano, N. Itaco, and T. T. S. Kuo, Prog. Part. Nucl. Phys. **62**, 135 (2009).

[37] R. Machleidt, Phys. Rev. C **63**, 024001 (2001).

[38] B. F. Bayman, A. Covello, A. Gargano, P. Guazzoni, and L. Zetta, Phys. Rev. C **90**, 044322 (2014) and references therein.

[39] L. Coraggio, A. Covello, A. Gargano, and N. Itaco, Phys. ReV. C **72**, 057302 (2005).

[40] L. Coraggio, A. Covello, A. Gargano, and N. Itaco, Phys. Rev. C **73**, 031302(R) (2006).

[41] D. Entem and R. Machleidt, Phys. Rev. C **68**, 041001 (2003).

[42] H. Naïdja, F. Nowacki, and K. Sieja, Acta Phys. Pol. B **46**, 669 (2015).

[43] H. Naïdja, F. Nowacki, B. Bounthong, M. Czerwiński, T. Rzaca-Urban, T. Rogiński, W. Urban, J. Wiśniewski, K. Sieja, A. G. Smith, J. F. Smith, G. S. Simpson, I. Ahmad, and J. P. Greene. Phys. Rev. C **95**, 064303 (2017).

[44] H. Naïdja, F. Nowacki, and B. Bounthong, Phys. Rev. C **96**, 034312 (2017).

[45] H. Naïdja and F. Nowacki, EPJ Web of Conferences **193**, 01005 (2018).

[46] H. Naïdja and F. Nowacki, J. Phys. Conf. Series **966**, 012061 (2018).

[47] E. Caurier and F. Nowacki, Acta. Phys. Polonica **30**, 705 (1999).

[48] E. Caurier, G. Martinez-Pinedo, F. Nowacki, A. Poves and A.P. Zuker, Rev. Mod. Phys. **77**, 427 (2005).

[49] L. Coraggio, A. Covello, A. Gargano, and N. Itaco, Phys. Rev. C **87**, 034309 (2013).

[50] W. Urban, W. R. Phillips, N. Schulz, B. J. P. Gall, I. Ahmad, M. Bentaleb, J. L. Durell, M. A. Jones, M. J. Leddy, E. Lubkiewicz, L. R. Morss, A. G. Smith, and B. J. Varley, Phys. Rev. C **62**, 044315 (2000).

[51] J. Shergur, A. Wöhr, W. B. Walters, K.-L. Kratz, O. Arndt, B. A. Brown, J. Cederkall, I. Dillmann, L. M. Fraile, P. Hoff, A. Joinet, U. Köster, and B. Pfeiffer, Phys. Rev. C **71**, 064321 (2005).

[52] J. Shergur, B. A. Brown, V. Fedoseyev, U. Köster, K.-L. Kratz, D. Seweryniak, W. B. Walters, A. Wöhr, D. Fedorov, M. Hannawald, M. Hjorth-Jensen, V. Mishin, B. Pfeiffer, J. J. Ressler, H. O. U. Fynbo, P. Hoff, H. Mach, T. Nilsson, K. Wilhelmsen-Rolander, H. Simon, A. Bickley, and the ISOLDE Collaboration, Phys. Rev. C **65**, 034313 (2002).

[53] S. Ilieva, Th. Kröll, J.-M. Régis, N. Saed-Samii, A. Blanc, A. M. Brice, L. M. Fraile, G. de France, A.-L. Hartig, C. Henrich, A. Ignatov, M. Jentschel, J. Jolie, W. Korten, U. Köster, S. Lalkovski, R. Lozeva, H. Mach, N. Marginean, P. Mutti, V. Paziy, P. H. Regan, G. S. Simpson, T. Soldner, M. Thürauf, C. A. Ur, W. Urban, and N. Warr, Phys. Rev. C **94**, 034302 (2016).

[54] A. Gargano and G. De Gregorio, EPJ Web of Conferences **232**, 04006 (2020).

TABLE II. Transition energies (E_γ), relative γ-ray intensities (I_γ), and placements of γ rays emitted following the β decay of ^{138}Sb. The number in parentheses is an error in the last digit. Systematic uncertainties of 0.25 keV and 5% for E_γ and I_γ, respectively, are included. The relative intensity should be multiplied by a factor of 0.62(5) to obtain the absolute intensity per 100 decays. This factor is deduced by the ratio between the 460.8-keV γ-ray events and the total β-ray events after subtracting the backgrounds.

E_γ (keV)	I_γ (rel)[a]	$E_{\mathrm{level},i}$ (keV)	$E_{\mathrm{level},f}$ (keV)
61.6(3)[c]	29.0(55)[b]	61.6	0
442.9(3)	46.2(38)	903.7	460.8
460.8(3)	100(6)	460.8	0
535.5(4)	0.76(34)	1439.2	903.7
606.0(10)[c]	1.19(57)	606.0	0
608.0(10)[c]	3.13(79)	608.0	0
627.5(3)	4.16(74)	1531.2	903.7
633.3(3)[c]	3.19(71)	633.3	0
778.1(3)	3.69(97)	1681.8	903.7
798.9(4)[c]	3.9(18)	798.9	0
862.9(3)	5.83(98)	1766.6	903.7
870.0(3)	1.10(39)	1773.7	903.7
973.7(5)[c]	2.7(15)	973.7	0
998.3(4)[c]	2.8(11)	998.3	0
1007.1(3)	4.53(91)	1467.8	460.8
1120.3(3)	5.6(11)	1581.1	460.8
1135.4(4)	1.72(58)	2037.0	903.7
1137.3(4)[c]	1.76(60)	1137.3	0
1154.9(3)	5.87(98)	1615.7	460.8
1191.4(3)	2.99(76)	2093.1	903.7
1247.4(4)	1.81(70)	3365.2	2117.8
1273.4(3)	4.59(90)	1734.2	460.8
1317.1(4)	1.69(57)	2220.8	903.7
1429.2(4)	2.05(75)	1890.0	460.8
1452.0(5)	2.13(97)	1912.8	460.8
1463.6(4)	1.59(43)	2367.8	903.7
1467.6(4)	1.94(51)	1467.8	0
1501.2(4)	2.76(66)	1962.0	460.8
1504.2(5)	1.15(76)	2407.8	903.7
1542.3(4)	1.72(75)	2445.5	903.7
1574.2(3)	3.8(10)	2037.0	460.8
1630.3(4)	3.42(64)	2093.1	460.8
1656.9(4)	5.22(98)	2117.8	460.8
1718.2(4)	1.80(74)	2179.0	460.8
1900.3(4)	1.79(65)	2361.1	460.8
1907.4(3)	0.94(75)	2367.8	460.8
1984.2(7)	1.62(72)	2445.5	460.8
2437.9(4)	2.4(14)	3341.8	903.7
2704.5(6)	0.53(39)	3165.4	460.8
2881.3(8)	0.62(39)	3341.8	460.8

[a] The relative γ-ray intensity, I_γ, is normalized to the intensity of the 460.8-keV transition.

[b] I_γ reported here is the total γ-ray and internal conversion electron intensities, calculated assuming $M1$ multipolarity.

[c] γ-ray transitions observed following β-delayed neutron emission.

TABLE III. The calculated one-neutron spectroscopic factors coupled to the ground state ($C^2S(0^+)$) and the 2_1^+ state ($C^2S(2^+)$), and the percentage contribution of $\nu(f_{7/2})^3$ in the wave functions of ^{137}Te from the Napoli and N3LOP interactions. See text for details.

^{137}Te	$C^2S(0^+)$ (Napoli/N3LOP)	$C^2S(2^+)$ (Napoli/N3LOP)	$\nu(1f_{7/2})^3$ (%) (Napoli/N3LOP)
$7/2_1^-$	0.72/0.67	0.10/0.04	61/54
$7/2_2^-$	0.01/0.03	0.45/0.54	29/29
$5/2_1^-$	0.01/0.02	1.13/0.96	53/46
$5/2_2^-$	0.19/0.18	0.00/0.01	4/1
$3/2_1^-$	0.01/0.01	0.47/0.45	44/37
$3/2_2^-$	0.71/0.64	0.09/0.12	5/3
$1/2_1^-$	0.48/0.35		3/1
$9/2_1^-$	0.01/0.00	0.38/0.41	27/27
$9/2_2^-$	0.01/0.40	0.28/0.09	70/7
$9/2_3^-$	0.49/0.05	0.00/0.24	2/55
$11/2_1^-$		0.65/0.61	59/48

TABLE IV. Reduced transition rates $B(E2)$ in $e^2\mathrm{b}^2$, spectroscopic quadrupole moments Q_s in $e\,fm^2$, and dimensionless nuclear magnetic moments g-factors of ^{138}Te from the Napoli and N3LOP interactions.

^{138}Te	Napoli	Mod. Napoli[a]	N3LOP
$B(E2;0_1^+ \to 2_1^+)$	0.318	0.324	0.316
$B(E2;2_1^+ \to 4_1^+)$	0.155	0.164	0.162
$B(E2;4_1^+ \to 6_1^+)$	0.071	0.127	0.129
$B(E2;2_2^+ \to 3_1^+)$	0.074	0.097	0.156
$B(E2;3_1^+ \to 5_1^+)$	0.006	0.122	0.100
$B(E2;2_2^+ \to 4_2^+)$	0.010	0.021	0.055
$Q_s(2_1^+)/g(2_1^+)$	-47/0.21	-47/0.21	-49/0.30
$Q_s(4_1^+)/g(4_1^+)$	-68/0.20	-70/0.22	-69/0.32
$Q_s(6_1^+)/g(6_1^+)$	-34/0.05	-70/0.35	-80/0.55
$Q_s(3_1^+)/g(3_1^+)$	-1.0/0.06	-2.1/0.08	-3.9/0.13
$Q_s(5_1^+)/g(5_1^+)$	35/-0.10	35/-0.09	-47/0.18
$Q_s(2_2^+)/g(2_2^+)$	29/0.04	34/0.02	42/0.05
$Q_s(4_2^+)/g(4_2^+)$	34/-0.10	32/-0.06	0.04/0.07

[a] Napoli interaction with modified $\nu(1f_{7/2})^2$ matrix elements, see text for details.